Application of Immersed-Boundary Method on Heat-Transfer Problems

Renato Salgado
renato.salgado@tecnico.ulisboa.pt

Instituto Superior Técnico, Lisboa, Portugal

May 2022

Abstract

This work focuses on the thermal simulation capabilities of *SOL* using an immersed boundary method. In particular, on the interpolation of the relevant variables from the original solid boundary to the IB one. Two schemes for interpolation are studied, capable of imposing both temperature and heat flux temperature boundary conditions. The schemes are then verified for low-Reynolds 2D Taylor-Couette flow problems with heat transfer, while also having their theoretical order of accuracy verified. A mesh robustness study is conducted across both schemes and boundary conditions, using triangular, quadrilateral, and hexagonal meshes verifying full capability at handling these grid topologies. The methods are also employed in simulations using hybrid meshes, where the least squares interpolation method capabilities are demonstrated. This methodology proves that the linear method lacks the robustness necessary to handle grids with arbitrary connectivity. The least squares interpolation method was also used to simulate flow over a cylinder with heat transfer, employing sampling of Nusselt numbers across the surface of the solid boundary. After an enhancement was developed and introduced to the Neumann interpolation method, the achieved results were concordant with the relevant literature and with the body fit simulations developed in *SOL* as a benchmark. Overall, this work verifies *SOL* for heat transfer Taylor-Couette flow simulations using the immersed boundary method for up to second order both for Dirichlet and Neumann boundary conditions. Furthermore, it proved capable of solving more complex boundary heat transfer problems, with a Nusselt number evolution comparable with the literature.
Keywords: IB-Method, CFD, Heat Transfer, Interpolation Methods, Order of Accuracy

1. Introduction

Following the tendencies of the CFD branch, the objective of the present work is to explore and implement IB methods for conjugated heat problems in a pre-existing CFD software developed by *LASEF* at *Instituto Superior Técnico*. An extensive amount of published work was developed using this software, named *SOL*, but a brief description of its functioning as well as its capabilities is featured in the following chapters. Published work developed using SOL can be seen in [1, 2, 3].

The aim of this master thesis is to enhance and improve the IB method functionality of the software developed at *LASEF* - *SOL*. This projects consists of several implementations, tests, evaluations and verifications. These contributed to three major aspects: new capabilities of *SOL*, increased robustness of the code and further debugging of the software.

2. Background

The immersed-boundary method is becoming very popular among the CFD community as it allows for the solution of more complex problems. This complexity can come from the geometry of the solids – the more complex the geometry, the harder it is to compute the mesh for the solid – or the movement of the solid body – if the body is moving within time, its boundaries are changing position within time requiring a remeshing process at each time step iteration. [4, 5, 6]

When using the IB method, cells that contain only fluid are isolated from the rest of the domain. This division of the fluid domain forms the IB boundary – a delimitation of the shape of the solid following the trends of the mesh, independently of its type. The IB boundary will outline the IB cells and the solid domain. IB cells are cells that contain the interface solid-fluid. Figure 1 depicts a generic IB boundary considering a random solid geometry in 2D.

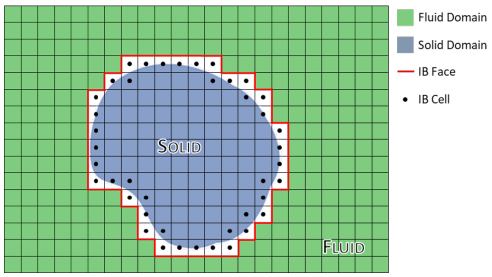

Figure 1: Generic representation of a 2D random solid geometry and its correspondent IB boundary.

The implementation of the IB method requires two major steps. The first step is when the entire mesh is analysed and the IB boundary is determined. Here, the fluid cells are isolated from IB cells (cells that contain vertices both in the fluid and solid domains) and solid cells. After the determination of the IB boundary, comes the second step of the IB method which is the transport variables interpolation from the solid surface boundary to the IB boundary. When using the IB method, the boundary conditions needed for solving the fluid bulk must be imposed at the IB boundary. Interpolation methods have to be used for the boundary conditions of the solid.

3. Interpolation Methods

3.1. Linear Method for Dirichlet Boundary Conditions

To linearly interpolate the temperature at the immersed boundary a ratio of distances must first be defined.

$$\eta = \frac{d_1}{d_1 + d_2} \tag{1}$$

Where d_1 and d_2 are defined as the distance from the IB face center to the fluid cell center of the cell containing the IB face and as the distance between the IB face center to the closest solid material point, respectively. These distances are schematized in Figure 2.

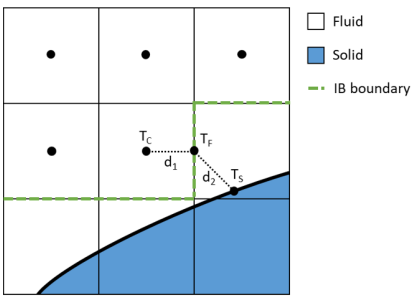

Figure 2: Definition of distances and location of interpolated values used in linear interpolation method for Dirichlet boundary condition.

The temperature at the IB face center can now be obtained with a weighted average using the calculated distance ratio.

$$T_f = T_c(1 - \eta) + \eta T_s \tag{2}$$

Where T_f is the interpolated temperature at the IB face center, T_c is the temperature at the fluid cell center which includes the IB face and T_s is the temperature at the closest solid point. These temperatures are also schematized in Figure 2.

3.2. Linear Method for Neumann Boundary Conditions

To linearly interpolate the temperature gradient at the immersed boundary the same ratio of distances defined on Equation 1 will be utilized.

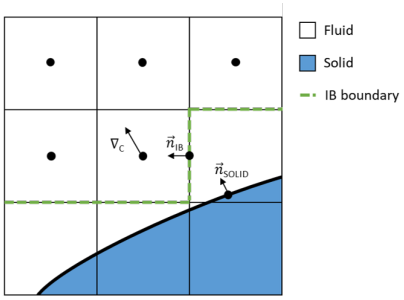

Figure 3: Definition of vectors and locations used in the linear interpolation method for Neumann boundary condition.

Figure 3 shows the vectors required for this interpolation. ∇_c represents the temperature gradient at the fluid cell center, $\vec{n}_{IB}$ is the unit length vector normal to the IB face pointing outwards from the solid body, and $\vec{n}_{SOLID}$ is the unit length vector normal to the solid body pointing outwards from the solid body.

Furthermore, two intermediary variables will be needed, ϕ_s and ϕ_c , which are defined as follows:

$$\phi_s = \nabla_T \cdot \vec{n}_{IB} \tag{3}$$

$$\phi_c = (\vec{n}_{IB} \cdot \vec{n}_{SOLID}) \times \left[\frac{dT}{dn}\right]_{SOLID} \tag{4}$$

Where $\left[\frac{dT}{dn}\right]_{SOLID}$ is the value of the normal temperature gradient at the solid boundary, this is, the Neumann condition being imposed at the solid boundary.

Finally, the value for the temperature gradient at the IB face center is calculated with a weighted average using the calculated distance ratio in an analogous manner to the linear temperature interpolation of Equation 2:

$$\phi_f = \phi_c(1 - \eta) + \eta \phi_s \tag{5}$$

Where ϕ_f is the temperature gradient for the IB face center.

3.3. Least Squares Interpolation Method for Dirichlet Boundary Conditions

This section details the methodology employed to interpolate a boundary condition for the IB face from an imposed temperature (Dirichlet BC) on the solid boundary, using a least squares methodology. The number of points considered varies depending on the local geometry. However, a generic situation is presented in Figure 4, where 5 neighbouring fluid cell centers, 4 IB face centers and 3 solid points are shown.

Figure 4: Schematic of relevant points for creation of the stencil in a generic face f.

In this case, the calculation of the value in face f, ϕ_f, uses a stencil consisting of 5 fluid cell (red dots) and 3 solid points (black dots). Each of these points represents a value for the temperature. No values from IB face centres are used for the interpolation.

A quadratic polynomial is now created for each point in the stencil, following the form:

$$\phi = \beta_0 + \beta_1 x + \beta_2 y + \beta_3 x^2 + \beta_4 y^2 + \beta_5 xy \quad (6)$$

Where the coefficients β_n are determined by the least square method and x and y represent the points' coordinates in the simulation's referential. In matrix form, this equation can be written as: $\phi = M\vec{\beta}$ where $\vec{\beta} = [\beta_0, \beta_1, \beta_2, \beta_3, \beta_4, \beta_5]^T$ and M :

$$M = \begin{bmatrix} 1 & x_1 & y_1 & x_1^2 & y_1^2 & x_1 y_1 \\ 1 & x_2 & y_2 & x_2^2 & y_2^2 & x_2 y_2 \\ \vdots & \vdots & \vdots & \vdots & \vdots & \vdots \\ 1 & x_n & y_n & x_n^2 & y_n^2 & x_n y_n \end{bmatrix} \quad (7)$$

Following the least squares method, minimizing the square of the difference between the values considered at each point corresponds to minimizing the value of $\|\phi - M\vec{\beta}\|^2$. Following the works of Kariya and Kurata [7] this minimization occurs when the calculation of the vector β is performed as follows:

$$\beta = \left(M^T \cdot M\right)^{-1} M^T \phi \quad (8)$$

After the β vector has been calculated, ϕ_f can be directly calculated using Equation 6.

3.4. Least Squares Interpolation Method for Neumann Boundary Conditions

This section details the methodology employed to interpolate a boundary condition for the IB face from an imposed temperature gradient (Neumann BC) on the solid boundary, using a least squares methodology.

The same generic detail of the IB cut presented in Figure 4 is considered. However, a new referential is used, centered on the solid point and using the solid points normal direction (vector $\vec{V_n}$) pointing outwards as the x direction and the tangential body direction (vector $\vec{V_t}$) as the y direction, as schematized in Figure 4. All points considered in this section use this referential.

In the generic case presented, 5 neighbouring fluid cell centers and 3 solid points are considered. The same quadratic polynomial as presented in Equation 6 is used for all fluid cell center points. However, the value inherited from solid points is a temperature derivative, forcing that the quadratic polynomial in Equation 6 must be differentiated with respect to x , the normal body direction, resulting in equation 9.

$$\phi = \beta_1 + 2x\beta_3 + \beta_5 y \quad (9)$$

Thus, the main difference from the methodology employed for Dirichlet boundary condition lies in the construction of matrix $M_{Neumann}$ as seen in Equation 10.

$$M_{Neumann} = \begin{bmatrix} 1 & x_1 & y_1 & x_1^2 & y_1^2 & x_1 y_1 \\ 1 & x_2 & y_2 & x_2^2 & y_2^2 & x_2 y_2 \\ \vdots & \vdots & \vdots & \vdots & \vdots & \vdots \\ 1 & x_n & y_n & x_n^2 & y_n^2 & x_n y_n \\ 0 & 1 & 0 & 2x_{n+1} & 0 & y_{n+1} \\ \vdots & \vdots & \vdots & \vdots & \vdots & \vdots \\ 0 & 1 & 0 & 2x_{n+m} & 0 & y_{n+m} \end{bmatrix} \quad (10)$$

Where n is the number of fluid cell centers in the stencil and m is the number of solid points in the stencil. Solving Equation 8 allows for the direct calculation of ϕ_f using Equation 9.

4. Taylor-Couette Problem

In order to perform the tests required, a physics problem geometry consisting of the two-dimensional flow between two cylinders was defined in *SOL*. This problem is also called a Taylor-Couette flow problem. All simulations in this chapter were conducted in stationary conditions, and meshes used in this chapter were hexagonal meshes.

The fluid domain in this problem corresponds to the space between the outer most cylinder with radius $R_0 = 1$ and and the inner most cylinder with

radius $R_{SOLID} = 0,5$. The outer most cylinder is stationary while the inner most cylinder is rotating with a constant angular velocity, $u_\theta = 1 rad/s$ in an anti-clockwise direction.

Regarding the temperature field; a Dirichlet boundary condition is applied on the outer wall, which is maintained at $T_0 = 0$. The boundary condition at the inner circle varies between different simulations. When a Dirichlet condition is applied, it has a value of $T_{SOLID} = 1$. When a Neumann boundary condition is applied, it has a value of $\left[\frac{dT}{dr}\right]_{r=R_{SOLID}} = 1$.

All Taylor-Couette simulations conducted use $Pr = 1$ and $Re = 0,25$.

After this physical domain is fully defined, the analytical solution for both velocity and temperature fields are implemented in *SOL*. This allows for the calculation of analytical errors for both the velocity and temperature fields given by each simulation.

4.1. Linear Method Results and Discussion

This section relates to the results for the temperature field obtained using the linear interpolation methods. Figure 5 shows the observed behaviour of the mean error for a mesh refinement study.

Table 1 represents the observed orders of accuracy for the linear interpolation methods, obtained in an analogous manner to trend line methodology used for the velocity field.

Table 1: Observed order of convergence using the linear interpolation method for both boundary conditions.

	Linear
Imposed Temperature (Dirichlet BC)	0,88
Imposed Temperature Gradient (Neumann BC)	1,20

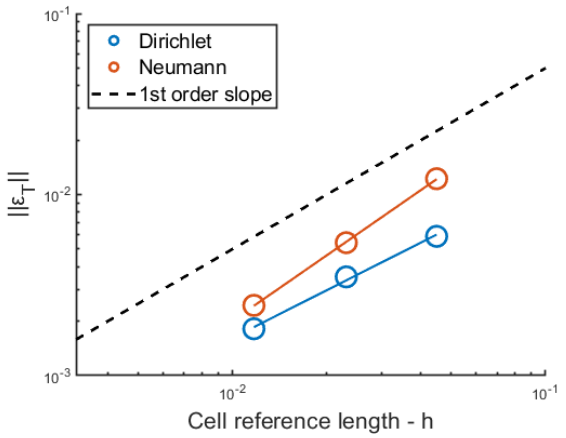

Figure 5: Error decay of the mean temperature error for a Taylor-Couette flow simulation.

Both schemes' observed order of accuracy are within an acceptable variance of the expected value of 1. The method for imposed temperature, despite having a deviation of 12% from the expected value, has lower analytical error in all considered meshes than the imposed temperature gradient method, despite it's considerably higher observed order of accuracy. The higher difference in the schemes' response for coarser meshes also points to the cause of the variance in order of accuracy. Since these methods present first degree order of accuracy, a mesh refinement study for a physical problem with coupling of the thermal and velocity fields would lead to a decrease of the velocity field calculation's order of accuracy. To address the need for a higher order thermal interpolation method, the least squares interpolation method is studied in the following section.

4.2. Least Squares Interpolation Method Results and Discussion

This section relates to the results obtained using the least squares interpolation method for the interpolation of the thermal boundary conditions at the IB boundary.

Figure 6 shows the resultant behaviour and Table 2 shows the observed order of accuracy.

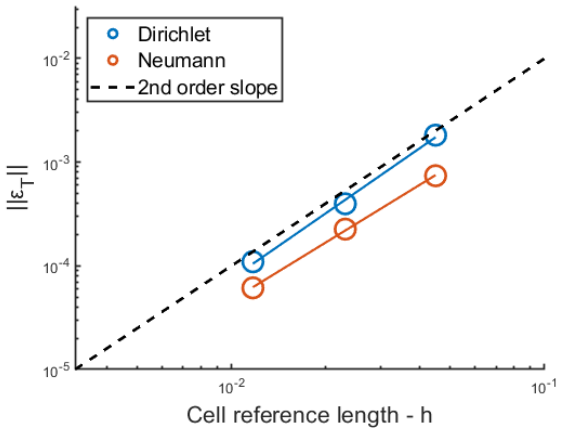

Figure 6: Error decay of the mean temperature error for a Taylor-Couette flow simulation with least squares interpolation method at the IB for Neumann and Dirichlet boundary conditions.

Table 2: Observed order of convergence using the least squares interpolation method for both boundary conditions.

	Least Squares
Imposed Temperature (Dirichlet BC)	2,09
Imposed Temperature Gradient (Neumann BC)	1,85

The least squares interpolation method's results present a similar situation to the linear methods' results since both boundary conditions' observed order of convergence have a maximum deviation

of 7.5% from the theoretical value of 2. This maximum deviation occurs for the Neumann boundary condition. The overall analytical error is an entire order of magnitude below that of the linear interpolation methods for most of the considered meshes, as is expected for higher order schemes. The least squares interpolation method also has a reasonably lower error when imposing temperature gradient rather than temperature. This difference is believed to be due to the gradient being able to immediately be implemented in the diffusive scheme and the temperature requiring an additional calculation. This hypothesis will be studied further in subsequent chapters.

5. Mesh Geometry Robustness Study

Testing the current capabilities of *SOL* at handling heat exchange over an immersed boundary using several different types of mesh and levels of refinement presents a invaluable opportunity to assess the robustness of both the interpolation methods developed and implemented.

SOL's response to this kind of testing can indicate both limitations in some methods' mesh handling and other methods' capabilities at solving the same problem. This knowledge enables an advantageous starting point for future simulations being employed using the optimal approach and optimal interpolation methodology selection.

All simulations in this chapter follow the same methodology described in Section 4 for the Taylor-Couette physical problem.

5.1. Structured Meshes

Three different types of structured meshes are considered for testing. The first type of meshes used are hexagonal, strictly structured in the fluid domain. The second type of structured mesh employed are triangular meshes, with some small variance in cell connectivity near the outer circle due to the body fitted nature of the mesh in regards to this outer boundary. The third and last type of mesh considered are fully structured radial quadrilateral mesh. For all types of meshes employed, three different levels of refinement were considered, corresponding to three different characteristic lengths.

5.1.1 Linear Interpolation Method Results and Discussion

All results are obtained using the linear interpolation method presented.

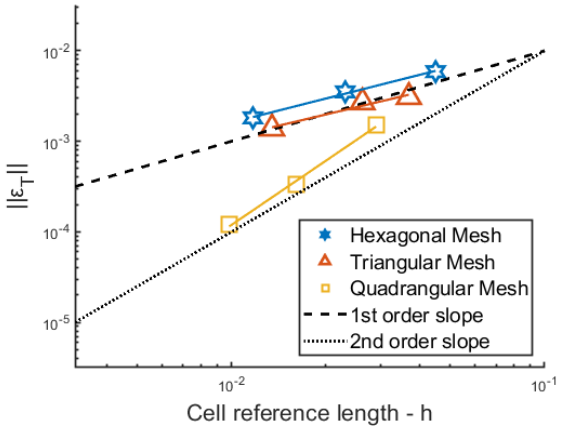

(a) Error decay with Dirichlet boundary condition

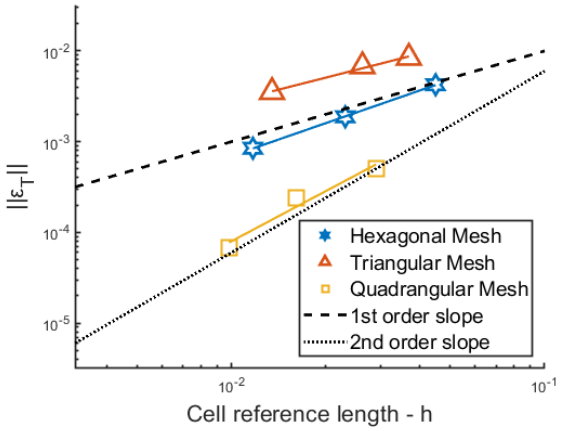

(b) Error decay with Neumann boundary condition

Figure 7: Observed error decay with linear interpolation method for various mesh types

Table 3: Observed order of convergence with linear method for three different meshes and boundary conditions.

	Triangular	Quadrilateral	Hexagonal
Imposed Temperature (Dirichlet BC)	0,82	2,35	0,88
Imposed Temperature Gradient (Neumann BC)	0,88	1,83	1,20

Figure 7 shows the observed behaviour for the considered methods, across both bondary conditions considered. Table 3 presents the observed order of accuracy for all studies presented in this section.

The mesh refinement studies conducted for the linear interpolation methods demonstrate a slight decrease in the observed order of accuracy when using triangular structured meshes compared to hexagonal ones, which is an expected result. The higher computational power required to mesh a geometry using hexagonal cells is well documented to improve accuracy of schemes over the easier to mesh triangular geometries. The observed order of accuracy for triangular meshes has a maxi-

mum deviation of 18% from the theoretical value of 1, which while considerable is compensated by a much easier meshing process, as mentioned. [8]

The major outliers are the results obtained when using quadrilateral radial meshes, where an observed order of accuracy much higher than the theoretical value of 1 is verified. Considering the exceptional quality these meshes possess for the current problem, as described in Chapter 5.1, these values do not point to a particularly capable scheme, but instead to a high sensibility to mesh quality. This hypothesis will be tested using hybrid meshes.

5.1.2 Least Squares Interpolation Method Results and Discussion

All results are obtained using the least squares interpolation method.

Table 4 presents the observed order of convergence for all studies presented in this section.

Table 4: Observed order of convergence with with least squares interpolation method for three different meshes and boundary conditions.

	Triangular	Quadrilateral	Hexagonal
Imposed Temperature (Dirichlet BC)	1,93	1,51	2,25
Imposed Temperature Gradient (Neumann BC)	1,78	2,28	1,85

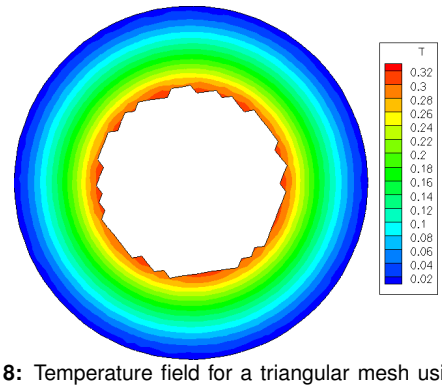

Figure 8: Temperature field for a triangular mesh using least squares interpolation method and a unitary Neumann boundary condition

The mesh refinement studies conducted for the least squares interpolation methods in this Section demonstrate a slight decrease in the observed order of accuracy when using triangular structured meshes compared to hexagonal meshes, which is an expected result which was also observed in the behaviour of the linear interpolation methods.

The major point to note is the result obtained when using quadrilateral radial meshes, where an observed order of accuracy half an order lower than the theoretical value of 2 is verified. This order of accuracy is in fact lower than that registered for the same meshes when utilizing a linear interpolation method. Considering the exceptional quality these meshes possess for the current problem, as described in Chapter 5.1, this behaviour points to a mesh geometry particularly optimal to implement the linear interpolation method, which resulted in an exceedingly higher order of accuracy than expected when using this method. Overall, these quadrilateral meshes observed behaviour is concordant with what was expected, with deviations due to it's particularly good fitting to the current physical problem and to linear interpolation methods.

It is worth noting that all three structured mesh types considered can be reused for conjugate heat transfer problems, with varying advantages. The higher coarseness inside the IB boundary for the hexagonal meshes would be of great value in conjugate heat transfer problems since the solid domain would represent a purely diffusive problem, which coupled with the much higher typical thermal conductivity of solids compared to that of fluids leads to the lower need for mesh refinement in this area. Complementarily, the radial quadrilateral meshes' internal boundary would be appropriate to represent, for example, an imposed heat flux typically associated with an electrical resistance, running through a solid submerged in a fluid onto which it is dissipating heat.

5.2. Hybrid Meshes

Hybrid meshes have a much wider range of connectivity compared to the previously considered structured meshes. While most elements on these grids are quadrilaterals, triangles also occur, resulting in the number of cells each vertex belongs to varying, from 3 to 5. These meshes characteristics lead to a higher difficulty for the interpolation methods at the IB boundary to function at the expected order of accuracy.

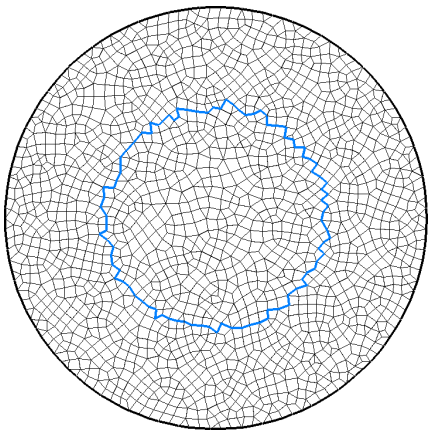

Figure 9: Example of a hybrid mesh used for robustness testing. The IB boundary is represented in blue. The outer circle, a body-fitted boundary, is represented in black

Five hybrid meshes of similar geometry but varying levels of refinement were considered. Figure 9 shows one such mesh, the second coarsest. This figure also demonstrates the higher complexity of the IB boundary.

5.2.1 Results and Discussion

Figure 10 shows the observed behaviour, and Figure 11 presents the temperature field obtained when utilizing a Neumann boundary condition and a least squares interpolation method.

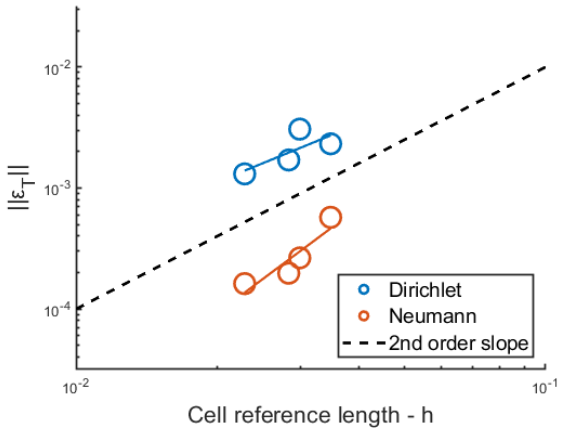

Figure 10: Observed error decay with least squares interpolation method for hybrid meshes

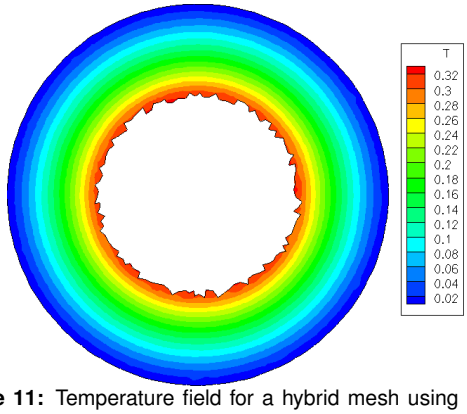

Figure 11: Temperature field for a hybrid mesh using a least squares interpolation method and an unitary Neumann boundary condition

Table 5: Observed order of convergence in hybrid meshes.

	Linear	Least Squares
Imposed Temperature (Dirichlet BC)	-0,37	1,59
Imposed Temperature Gradient (Neumann BC)	-4,02	2,89

Firstly, the results obtained when using the linear interpolation method show a complete lack of sensitivity of the mean temperature error in regards to mesh refinement, pointing to a high degree of mesh sensitivity, as evidenced in Table 5. These methods are not considered capable of handling hybrid mesh geometries, and are discouraged from being used outside of structured mesh types.

The least squares interpolation method shows variable robustness when handling hybrid meshes. When imposing a temperature gradient at the solid boundary, the observed order of accuracy is in fact higher than the theoretical value of 2. However, when imposing temperature the observed order of accuracy experiences a decrease of 21% regarding the expected second order behaviour. It is known that when the maximum error for the temperature field has no variation across a mesh refinement study, the order of accuracy of the mean error lowers by at least 1. The hypothesis that this phenomenon is occurring was verified by analysing the maximum error distribution.

Overall, the developed least squares interpolation method for thermal interpolations at the immersed boundary is robust and capable of handling hybrid meshes. A boundary condition of imposed temperature gradient (Neumann) appears to be the optimal way to implement boundary conditions using this method.

6. Heat Transfer on the Surface of a Cylinder

The fluid domain comprises a rectangular geometry with one inlet on which flow enters the geometry with horizontal free stream velocity $U_0 = 1$, null vertical velocity and temperature $T_0 = 0$ and one outlet with $p = 0$ and null velocity derivatives. Both bottom and top walls have a $T_{WALL} = 0$ Dirichlet boundary condition and no permeability, this is, null vertical velocity.

All simulations conducted use $Pr = 0.7$ and $Re = 20$.

Simulations utilizing the body fit approach are also performed in this section as a means of benchmarking the IB results.

The Nusselt number is calculated and sampled along the cylinder boundary for both IB and body fit simulations and is the variable of most importance to the current study.

6.1. Dirichlet Results and Discussion

Figure 12 shows the resultant temperature field across the entire fluid Domain when utilizing a Dirichlet boundary condition on the cylinder surface.

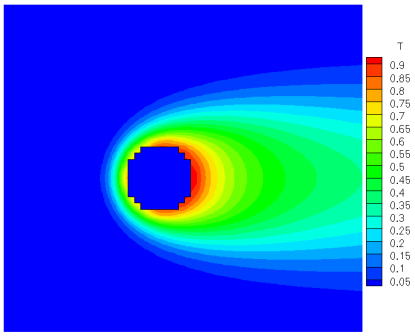

Figure 12: Detail of temperature field for cylinder with Dirichlet BC using IB method and a mesh with $h = 0.1$.

13 compares the results from the most refined mesh to the results obtained in *SOL* using a body fit approach and to the literature data obtained by Zhang in [9].

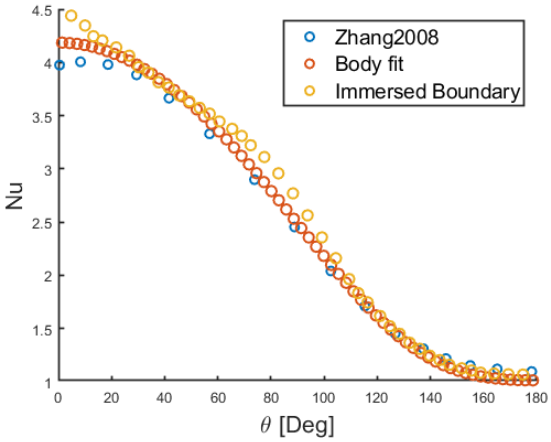

Figure 13: Comparison of Nusselt number distribution over surface of cylinder using IB method, Body Fit method and literature data.

The IB results present a high concordance with both the literature data and the body fit results. The most noteworthy variance between the data is an overshoot at the leading edge of the cylinder when considering the IB method, which also occurs with the bodyfit approach with a lower magnitude.

A mesh with a bigger fluid domain size is considered to analyse confinement effects on the Nusselt overshoot visible in comparison to the literature. The simulation preserves all other characteristics of the simulations performed so far in this section. No improvement to the overshoot is verified.

6.2. Neumann Results and Discussion

Figure 14 evidences the non-symmetric flow resultant from utilizing the existing Neumann interpolation method in the simulation of the current physical problem.

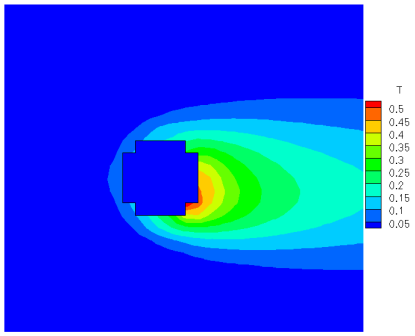

Figure 14: Detail of temperature field for cylinder with Neumann BC using IB method with coarsest mesh.

Considering the unexpected and erroneous nature of these results for all mesh refinements considered, no further results that utilize this Neumann interpolation method for the IB boundary are presented. These results indicate an error is occurring in the Neumann least squares interpolation method used. Chapter 7 addresses this limitation.

7. Modified Neumann Interpolation Methods

7.1. IB Face Centered Referential

The previously defined method defines the main point in the stencil as the main solid point. This point is used as the origin of the referential, from which all distances are measured and, more importantly, it dictates the main directions, defined as it's normal and tangent vectors.

Figure 15 demonstrates the new coordinate system used, where $\overrightarrow{V_n}$ and $\overrightarrow{V_t}$ represent the base vectors of the new coordinate system, corresponding in the relevant equations to, respectively, x and y. Variables represented in this referential are identified by the subscript $Local$.

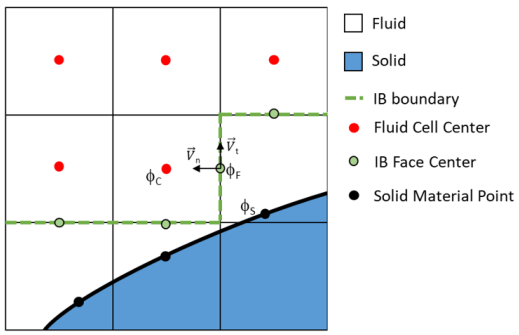

Figure 15: Schematic of points and vectors for modified Neumann interpolation method.

This reference system does not address the inherent error associated with assuming the solid point normal vectors and the IB face normal vector share the same direction. However, the main advantage in utilizing an IB face centered referential lies in the much simpler calculation of the desired

variable: the temperature gradient at the IB face center. Since the referential used has the main direction defined by the normal unit vector to the IB face center, the gradient at this point can be directly calculated in the direction of the IB face center normal.

7.1.1 Results and Discussion

Figure 16 shows the Nusselt distribution along the cylinder when using a IB face centered Neumann interpolation method using the finest mesh considered.

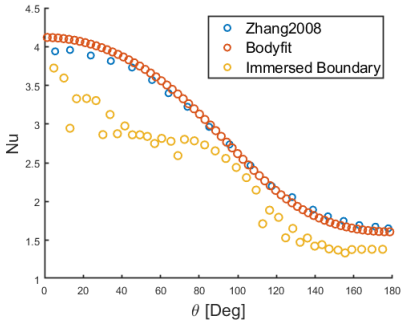

Figure 16: Comparison of Nusselt distribution obtained using IB method, a body fit approach and literature data.

Despite the method proving capable of achieving a solution macroscopically similar to that of the body fit approach, a more thorough analysis of the heat transfer across the surface of the cylinder, presented as the Nusselt distribution, demonstrates that even for the most refined meshes a substantial deviation from the expected results presented by the literature occurs. This methodology is further improved in the next section.

7.2. Combination of Directional Derivatives

The previous methodology assumes that the IB face center normal and the solid face normal vectors share the same direction. The inability to account for the different vector directions lead to the development of the methodology presented in this section. To address this limitation, a weighted combination of both derivatives is utilized. Each derivative's relative weight is defined as the value of the unit length vector upon which the temperature gradient occurs, when defined in the local coordinate system as defined in Section 7.1. Using this approach, each polynomial imposes the correct temperature gradient, at the correct relative location, imposed in the correct direction. Equation 11 defines this process.

$$\frac{dT}{d\overrightarrow{n}} = n_x \frac{d\phi}{dx} + n_y \frac{d\phi}{dy} \tag{11}$$

where $\overrightarrow{n}$ is the unit length vector upon which the temperature gradient is applied. The variables n_x and n_y correspond to the coordinates of vector $\overrightarrow{n}$ in the local coordinate system as defined in Section 7.1, as shown in Equation 12.

$$\overrightarrow{n} = (n_x; n_y)_{Local} \tag{12}$$

For the solid points considered in this work, $\overrightarrow{n}$ is simply the outwards pointing unit length body normal.

7.2.1 Results and Discussion

The behaviour achieved with the addition of a combination of directional derivatives to the Neumann interpolation method grants a response of the local heat transfer across the surface of the cylinder with a much higher concordance to the literature data. These results prove the postulated hypothesis that the deviation from the literature data and the body fit data was mostly due to the previous interpolation not addressing the difference in normal vectors direction.

Figure 17 compares the Nusselt distribution in literature data from Zhang2008 [9], with the distribution obtained using the IB method in *SOL* and with the results achieved using a body fit approach also using *SOL*.

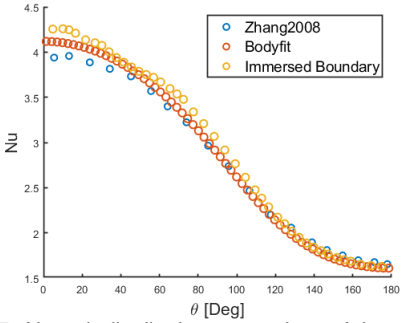

Figure 17: Nusselt distribution comparison of the results from the IB method, a body fit approach and literature data.

The Immersed Boundary results utilizing the combination of direction derivatives achieve a very high concordance with the results also obtained in *SOL* utilizing a body fit approach. However both these methodologies differ from the literature data at the leading half of the cylinder, culminating in the leading stagnation point, where a slight overshoot, of approximately 12% for the IB method and 8% for the body fit method, occurs. This effect is also observed for the Dirichlet results, and is believed to occur due to differing effects of confinement when comparing the simulation obtained in *SOL* from those conducted by Zhang in [9], be it due to different domain size, or slightly different boundary conditions.

The results indicate there are benefits in utilizing Neumann boundary conditions instead of Dirichlet.

Figures 13 and 17 show a higher concordance with the data obtained with the body fit methodology when imposing heat flux.

8. Conclusions

The present work focused on the thermal simulation capabilities of *SOL* using the immersed boundary method. The overall goal was to enable the software to simulate heat transfer problems using the IB method. In particular, the work focused on the interpolation of the relevant variables from the original solid boundary to the IB boundary. After this work, *SOL* is capable of handling both imposed temperature and imposed heat flux temperature boundary conditions across physical problems of varying complexity and using different mesh geometries.

Both linear and least squares interpolation methods were verified in both boundary cases using analytical data for low-Reynolds 2D Taylor-Couette flow problems with heat transfer, while also verifying their theoretical order of accuracy.

An extensive study of the developed methods was conducted using various types of structured grids across a range of refinement. The code showed robustness to variable mesh geometries for both methods using Dirichlet and Neumann boundary conditions.

Several simulations using hybrid meshes for Taylor-Couette flow problems were also performed, revealing an inability of the linear interpolation method in handling grids with more irregular connectivity. The same methodology was also used to demonstrate the least squares interpolation method's ability to handle these mesh geometry.

The least squares interpolation method was used in simulating flow over a cylinder with heat transfer, employing sampling of Nusselt numbers across the surface of the IB boundary. The same physical problem was also simulated using a body fit methodology, in order to obtain data also provided by *SOL* to use as benchmark for the IB method's results.

The Dirichlet boundary condition proved capable of achieving results that were in accordance with both the literature and the body fit approach. However, this study revealed that the least squares interpolation method for Neumann boundary conditions was not capable of handling this more complex simulation. This Neumann interpolation method limitation was addressed in two ways, by changing the coordinate system used while constructing the stencil, and by enabling the imposition of temperature gradients upon any direction by utilizing a combination of directional derivatives. These alterations proved capable of resolving the method limitations discovered, with the Neumann interpolation method achieving results with high concordance with the literature data and with the body fit approach.

Overall, *SOL* was verified using analytical data for heat transfer Taylor-Couette flow simulations using the immersed boundary method for up to second order across both Dirichlet and Neumann boundary conditions, opening the possibility for future work to implement fully conjugate heat transfer problems.

The current work furthers the capabilities of *SOL* such that future work may continue to expand upon the IB method range of operations.

References

[1] J. Alexandre, "A 2-D Immersed Boundary Method on Low Reynolds Moving Body," *MSc thesis*, 2014.

[2] D. Martins, "On the suppression of spurious pressure oscillations in immersed boundary methods with unstructured grids," *MSc thesis*, 2016.

[3] H. Daniel, "Error Estimation Criteria to Couple the Immersed Boundary Method with an Automated Adaptive Grid Algorithm," *MSc thesis*, 2017.

[4] T. Kajishima and K. Taira, "Immersed Boundary Methods," *Computational Fluid Dynamics*, 2017.

[5] S. Roy, A. De, and E. Balaras, "Immersed Boundary Method: Development and Applications," 2020.

[6] C. Santarelli, T. Kempe, and J. Fröhlich, "Immersed boundary methods for heat transfer," *International Journal of Numerical Methods for Heat and Fluid Flow*, vol. 26, mar 2016.

[7] T. Kariya and H. Kurata, "Generalized Least Squares," *Generalized Least Squares*, vol. 7, 2004.

[8] I. Sadrehaghighi, "Mesh Generation in CFD," 2020.

[9] N. Zhang, Z. C. Zheng, and S. Eckels, "Study of heat-transfer on the surface of a circular cylinder in flow using an immersed-boundary method," *International Journal of Heat and Fluid Flow*, vol. 29, no. 6, 2008.